Layer-by-layer assembled multilayer of graphene/Prussian blue toward simultaneous electrochemical and SPR detection of H_2O_2

Yan Mao [a], Yu Bao [a,*], Wei Wang [a], Zhenggang Li [a], Fenghua Li [a], Li Niu [a,b,**]

[a] Engineering Laboratory for Modern Analytical Techniques, c/o State Key Laboratory of Electroanalytical Chemistry, Changchun Institute of Applied Chemistry, Graduate University of the Chinese Academy of Sciences, Chinese Academy of Sciences, Changchun 130022, Jilin, PR China
[b] Department of Chemistry and NanoDTU, Technical University of Denmark, DK-2800 Kgs, Lyngby, Denmark

ARTICLE INFO

ABSTRACT

A new type of chemically converted graphene sheets, cationic polyelectrolyte-functionalized ionic liquid decorated graphene sheets (PFIL–GS) composite, was synthesized and characterized by Ultraviolet–visible (UV–vis) absorption, Fourier transform infrared, and Raman spectroscopy. It was found that the presence of PFIL enabled the formation of a very stable aqueous dispersion due to the electrostatic repulsion between PFIL modified graphene sheets. With respect to the excellent dispersibility of this material, we have fabricated a novel PFIL–GS/Prussian blue (PB) nanocomposite multilayer film via classic layer-by-layer (LBL) assembly. The assembly process was confirmed by UV–vis spectroscopy and surface plasmon resonance (SPR) spectroscopy, which showed linear responses to the numbers of the deposited PFIL–GS/PB bilayers. Moreover, the as-prepared composite films were used to detect hydrogen peroxide (H_2O_2) by electrochemical surface plasmon resonance (EC-SPR) spectroscopy. This real time EC-SPR technique can provide simultaneous monitoring of both optical SPR signal and electrochemical current responses upon injecting H_2O_2 into the reaction cell. The experimental results revealed that both the electrochemical and SPR signal exhibited splendid linear relationship to the concentration of the injected H_2O_2, and the detection limit could be up to 1 μM.

© 2011 Elsevier B.V. All rights reserved.

1. Introduction

Graphene, a new class of two-dimensional carbon nanostructure, has attracted extensive attention from the physics, chemistry, and materials science communities [1] since Geim et al. first isolated single-layer samples from graphite in 2004 [2]. This material holds great promise for potential applications in many technological fields (e.g. nanocomposite, lithium ion batteries, solar cells, etc.) [3–5]. Recently, this material also attracts great interest in electrochemical sensors and biosensors [6,7], owing to its high conductivity at room temperature [8]. However, most unique properties of graphene sheets are only associated with individual sheets. Consequently, the key challenge in the synthesis and processing of bulk-quantity graphene sheets is aggregation deriving from high cohesive *van der Waals* energy [9]. In order to overcome this problem, functionalization of graphene sheets becomes a major strategy for improving their solubility and self-assembly properties [10]. One approach is based on the π–π interactions of the chemically converted graphene sheets (CCG) with conjugated polymers or aromatic molecules such as polyvinylpyrrolidone [11], sulfonated polyaniline [12], and polyelectrolyte [13]. In these cases, the sulfonated conjugated polymers and the decorated aromatic molecules function as anionic dispersants during the reduction of graphene oxide (GO). The conjugated moieties provide strong affinity with the sp^2 domains of CCG sheets via π-stacking, while the anionic moieties provide electrostatic repulsion to stabilize the resulting functionalized CCG sheets in aqueous dispersions. The other approach is grafting some molecules (e.g. octadecylamine [10], aryl diazonium salts [14], or isocyanate [15]) on to graphene sheets according to covalent reactions. In our previous works, Yang [16] reported polydisperse CCG that were covalently functionalized with ionic liquid. Meanwhile, many graphene-based nanocomposites have been designed toward applications in electrochemical sensors [6,17]. The development of a polyelectrolyte-functionalized ionic liquid (PFIL) has been previously reported by covalent attachment of an ionic liquid unit onto polyethylenimine (PEI) [18]. PFIL has already been used as a film to enhance the electrochemical response (e.g. good electrochemical properties of PFIL-modified electrode

* Corresponding author. Fax: +86 431 8526 2800.
** Corresponding author at: Engineering Laboratory for Modern Analytical Techniques, c/o State Key Laboratory of Electroanalytical Chemistry, Changchun Institute of Applied Chemistry, Graduate University of the Chinese Academy of Sciences, Chinese Academy of Sciences, Changchun 130022, Jilin, PR China.
Fax: +86 431 8526 2800.
E-mail addresses: ybao@ciac.jl.cn (Y. Bao), lniu@ciac.jl.cn, lniu@kemi.dtu.dk (L. Niu).

in a supporting electrolyte-free solution [19], good electrocatalytical activity toward the reduction of hydrogen peroxide [20], etc.).

Among multifarious biosensors, hydrogen peroxide (H_2O_2) as an important intermediate species or product has been exhibited in many biological and environmental processes. The detection of H_2O_2 plays a significant role in many fields including clinic, food, pharmaceutical and environmental analysis [21]. Hitherto, a variety of quantitative methods have already been developed for the detection of H_2O_2. The most commonly used approaches are spectrometry [22], chemiluminescence [23], and electrochemistry [24]. Surface plasmon resonance (SPR) spectroscopy is a versatile tool to probe refractive index changes occurring on thin metal films as a result of recognition events or chemical reactions [25]. However, very few H_2O_2 sensors are fabricated on the basis of SPR spectroscopy [26]. Because of minute and nonspecific changes in refractive index, it is often difficult to directly detect molecules with low molecular weights in practical SPR sensing applications [27].

In this work, a novel PFIL functionalized graphene sheets (PFIL–GS) nanocomposite was synthesized, and it could form a very stable aqueous dispersion. As known to all, Prussian blue (PB) can reduce H_2O_2 at a very rapid catalytic rate with a low overpotential [28], and layer-by-layer (LBL) assembly is widely used as a powerful and versatile method for the preparation of ultrathin multilayer films [29]. Thus, the use of PFIL–GS and PB nanoparticles (PB NPs) as building blocks for constructing 3D nanocomposite films was achieved via LBL assembly method. Based on the high conductivity of GS and the excellent electrocatalytical activity toward H_2O_2 of PB, the as-prepared composite films were used as substrates of EC-SPR spectroscopy toward H_2O_2 detection. Upon injecting H_2O_2 into the reaction cell, optical SPR signals and electrochemical current responses are simultaneously monitored in real time, and the analytical performances have been discussed. This simultaneous detection method can provide dual information to improve the reliability of the test results.

2. Experimental

2.1. Reagents

Graphite powder (spectral requirement) was purchased from Shanghai Chemicals. Hydrazine solution (50% in water) and potassium chloride (KCl, ≥96.0%) were obtained from Beijing Yili Chemicals. Ammonia solution (25% in water), potassium ferricyanide ($K_3Fe(CN)_6$, ≥99.5%) and hydrogen peroxide (H_2O_2, ≥30%) were obtained from Beijing Chemicals. Ferrous chloride ($FeCl_2 \cdot 4H_2O$, ≥99.5%) was purchased from Yueqiao Chemicals. 3-Mercaptopropionic acid (99%) was purchased from Alfa Aesar. Ascorbic acid (AA) was purchased from Fluka. Dopamine hydrochloride (DA) and uric acid (UA) were obtained from sigma. Cysteine (Cys) and glutathione (GSH) were purchased from China Huishi Biochemicals. All chemicals were of analytical grade and used as received. All aqueous solutions were prepared with ultrapure water (>18 MΩ cm) obtained from Millipore system.

2.2. Instrumentation

Ultraviolet–visible (UV–vis) absorption spectra were recorded using a CARY 500 Scan UV/vis/NIR spectrophotometer. Fourier transform infrared spectra (FTIR) were recorded on a Bruker Vertex 70 spectrometer ($4\,cm^{-1}$). Raman spectra were collected using a Renishaw 2000 system (Renishaw Ltd., U.K.) with an argon ion laser (514.5 nm) and a charge-coupled-device detector. Zeta potential was recorded on a Malvern Nano-ZS Instrument. Scanning electron microscopy (SEM) images were obtained from an XL30 ESEM

FEG scanning electron microscope operating at 20 kV. Transmission electron microscopy (TEM) image was obtained using a Hitachi H600 transmission electron microscope operating at 100 kV.

SPR measurements and EC-SPR measurements were performed using an EC-SPR spectrometer (DyneChem, China). As shown in Scheme 1, the setup of the electrochemical SPR cell was designed specially to drive SPR and electrochemistry "in situ". The method used for surface plasmon detection was attenuated total reflectance (ATR) spectroscopy. Surface plasmon spectroscopic data were collected using Kretschmann optical configuration. The glass slide with the evaporated gold on the opposite side was pressed on a ZK_7 cylindrical glass prism via an index matching liquid. The gold surface of the slide was covered with silicone rubber sheet with a hole for the electrolyte contact. A 5 mW diode laser ($\lambda = 670$ nm) was focused through a prism (ZK_7) onto the film, and the reflected beam was detected by a bi-cell photodiode instead of the widely used linear diode array or charge coupled device (CCD). In these EC-SPR measurements, the gold substrate that carried the optical surface mode was simultaneously used as the working electrode in electrochemical experiments. The electrochemical experiments were provided with a platinum wire auxiliary electrode and a KCl saturated Ag|AgCl reference electrode in an integrated electrochemical analyser (DyneChem, China).

2.3. Preparation of GO and GS

GO was synthesized from natural graphite powder following a method reported by Kovtyukhova et al. [30] with slight modifications. GS was synthesized via the method presented by Li et al. [31]. Briefly, 10 mL of GO homogeneous dispersion (in water, 0.05 wt%) was mixed with 10 mL of water, 80 μL of ammonia solution and 7 μL of hydrazine solution in a 50 mL glass vial. The resulting mixture was held at 95 °C for 1 h under vigorous agitation, and then the GS solution was obtained.

### 2.4. Synthesis of PFIL and PFIL–GS

PFIL was prepared following our previous report [18], and the molecular structure was illustrated in Scheme S1. 40 mg of PFIL was added to 20 mL of the GO dispersion, and then stirred at 50 °C overnight. After cooled to room temperature, ammonia solution was added to the reaction solution to increase the pH value around 10, then 14 μL of hydrazine solution was added. After being stirred for a few minutes, the GO was reduced to GS by putting the mixture in an oil path (~95 °C) for about 1 h, and then a homogeneous black dispersion was obtained. The dispersion was filtered through a nylon membrane (0.22 μm pore size) and was repeatedly washed with water, then redispersed in the water to obtain PFIL–GS aqueous dispersion.

2.5. Synthesis of PB NPs

PB NPs were synthesized according to DeLongcham's method [20,32]. Briefly, 35 mL of 0.01 M $FeCl_2$ aqueous solution was added dropwise to a 35 mL of 0.05 M $K_3Fe(CN)_6$ solution containing 0.05 M KCl. The dialysis process was used to remove the large excess of $K_3Fe(CN)_6$ and KCl. In order to obtain a stable dispersion, the dialysis procedure was carried out at least 5 days.

2.6. Preparation of LBL films

The quartz substrates were boiled for 30 min in a freshly made *Piranha* solution (H_2SO_4/H_2O_2, v/v, 3/1), following by ultrasonic cleaning for 3 times with distilled water. After treatments, quartz substrates were rich in negative charges. Before use, the gold chips were immersed in 10 mM 3-mercaptopropionic acid ethanol
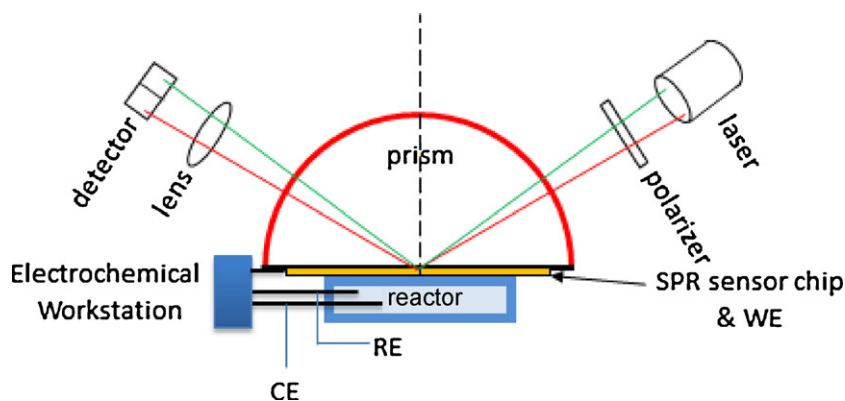
Scheme 1. Scheme of EC-SPR setup.

solution overnight. Quartz substrates and gold chips were firstly immersed into PFIL–GS aqueous solution for 30 min to form a positively charged surface, then washed three times with distilled water. The slides were then exposed to the negatively charged PB NPs aqueous solution for 30 min, and washed three times with distilled water. This cycle made one bilayer of PFIL–GS and PB, denoted as (PFIL–GS/PB). The cycle was repeated to obtain the desired number of bilayers.

3. Results and discussion

3.1. Spectral characterization of the PFIL–GS

The preparation procedure of PFIL–GS is illustrated in Scheme 2. The PFIL was coupled on graphene sheets through not only the electrostatic interactions between the positively charged imidazole ring of PFIL and the negatively charged carboxylic acid groups on graphene sheets [31], but also the weak π–π interactions between the imidazole ring of PFIL and the aromatic rings of graphene sheets.

UV–vis absorption, FTIR, and Raman spectra were used to illustrate the structure changes of graphene sheets before and after reduction. The absorption in the UV spectra of GO, GS, and PFIL–GS are 230 nm, 266 nm and 266 nm, respectively (as shown in Fig. 1), which means that the electronic conjugation within the graphene sheets is restored upon reduction [31]. The inset photograph shows that the color of the solution turns from pale brown to black,

further confirming the reduction process. The UV–vis results are corroborated by the FTIR results, as shown in Fig. 2. For the GO film, the C=O peak in the carboxylic acid and carbonyl moieties is at 1728 cm^{-1}. The peak at 1588 cm^{-1} can be assigned to the vibrations of the residual water, but may also contain components from skeletal vibrations of unoxidized graphitic domains [15]. After the reduction with hydrazine, the FTIR spectra of GS is essentially featureless except the C=C conjugation and C–C bands at 1535 cm^{-1} and 1190 cm^{-1}, respectively. Two characteristic peaks at 1652 cm^{-1} and 1446 cm^{-1} assign to the vibrations of amide I and amide II in the spectrum of PFIL, which are consistent with the previous report [18]. As seen from the PFIL–GS spectra, the amide I and amide II vibrations are still observed, indicating the presence of PFIL component. However, the absorption peaks shift to 1657 cm^{-1} and 1449 cm^{-1}, which might be attributed to the π–π stacking between PFIL and GS. And the peak at 1572 cm^{-1} is attributed to the stretching of C=C bonds of GS restored upon hydrazine reduction [33]. The peak at 1728 cm^{-1} disappears, which demonstrate that GO is triumphantly reduced to GS. Further evidence for the formation of PFIL–GS composite can be provided by Raman analysis (see Fig. S1 in the supporting information). The Raman spectrum of GO shows two broad peaks at 1353 and 1603 cm^{-1}, which corresponding to the D- and G-bands of graphene individually. After GO is chemically reduced to GS, the D-band and G-band peaks become narrower and G-band shifts to 1601 cm^{-1}, with an increase in the D/G intensity ratio compared to that observed in GO. The increase of the D/G intensity ratio suggests that the average size of the sp^2 domains is
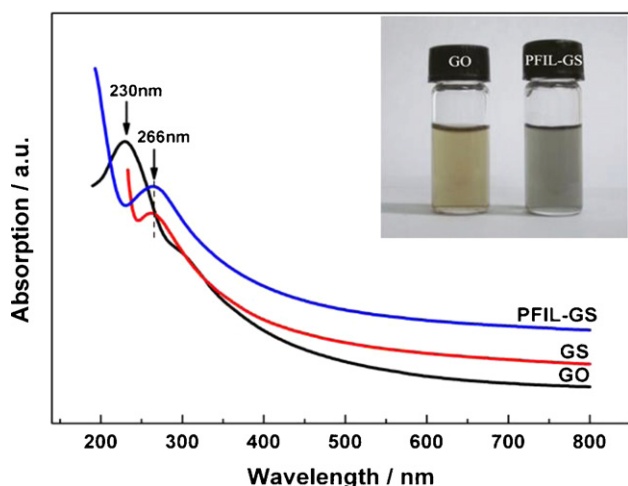

Fig. 1. UV–vis spectra of GO, GS and PFIL–GS solutions. Inset: a photograph of GO and PFIL–GS nanocomposite solutions.
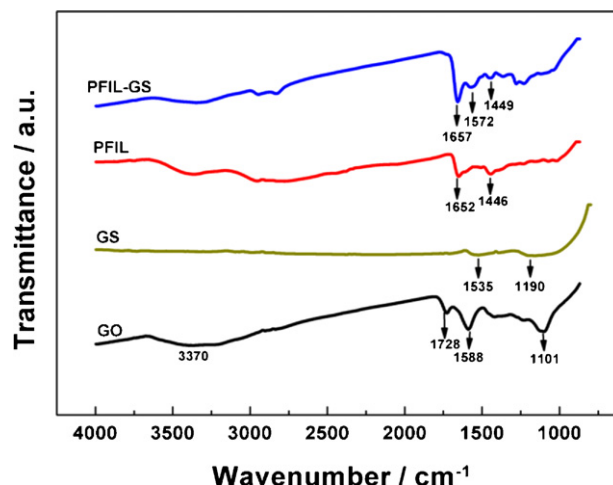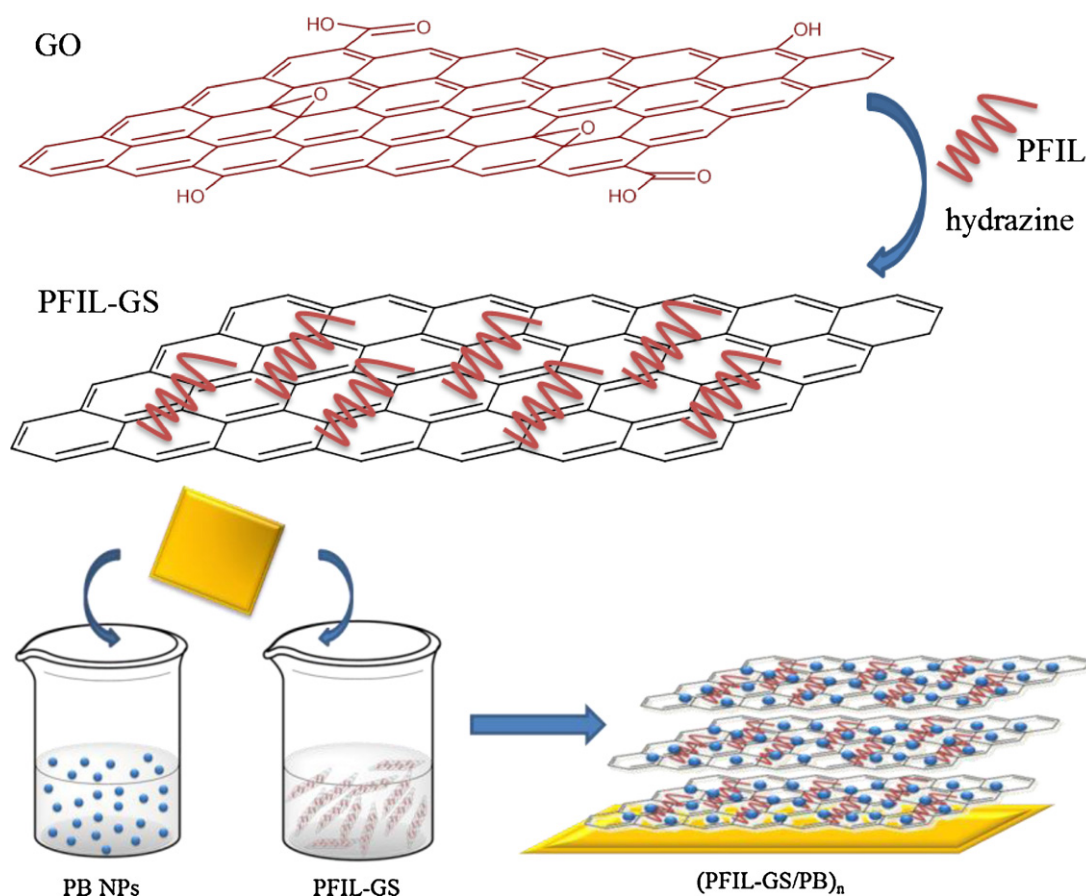

Fig. 2. FTIR spectra of GO, GS, PFIL, and PFIL–GS composites.

Scheme 2. Schematic diagram of the synthesis of PFIL–GS and assembly process of PFIL–GS and PB NPs.

decreased upon reduction of the GO sheets [34]. The *zeta* potential of PFIL–GS is +39.8 mV, which means that the PFIL–GS are positively charged. As a result, the PFIL–GS could be stably dispersed in water for more than 3 months due to the electrostatic repulsion.

3.2. Characterization of PB nanoparticles

The stable blue PB dispersion was produced, which was characterized by UV–vis absorption spectroscopy and TEM (see Fig. S2 in the supporting information). A broad absorption peak is clearly observed at 688 nm ascribing to the intervalence charge transfer band of PB NPs [20]. TEM image of the resulting PB particles shows spherical nanostructure with ca. 35 nm diameters and a relatively narrow size distribution.

3.3. LBL assembly of (PFIL–GS/PB)$_n$

The assembly procedure of PFIL–GS and PB NPs is shown in Scheme 1. A (PFIL–GS/PB)$_n$ multilayer film could be formed with strong electrostatic interactions between positively charged PFIL–GS and negatively charged PB NPs. UV–vis spectroscopy has proved to be a useful and facile technique to evaluate the growth process of a multilayer film and was used in the present work to monitor the LBL assembly process of (PFIL–GS/PB)$_n$ multilayer film. Fig. 3 shows the UV–vis absorption spectra of the (PFIL–GS/PB)$_n$ multilayer film with different bilayer numbers. The PFIL–GS multilayer films show a broad absorption around 280 nm, which is the characteristic adsorption of the assembled graphene. The PB NPs in the multilayer films express an absorption peak at 673 nm which is originated from the charge transfer between Fe^{3+} and

Fe^{2+}. The broad adsorption of PFIL–GS in the 280 nm region and characteristic absorption of PB NPs at 673 nm can be utilized to determine the assembled materials in a given bilayer. The clear increase in the absorbance with the assembly step is indicative of the film deposition on the quartz substrate. In addition, the peak absorbance at 280 nm and 673 nm are increased linearly with the number of deposited PFIL–GS/PB bilayers with a correlation coefficient of 0.999, indicating the uniform growth of the multilayer films.
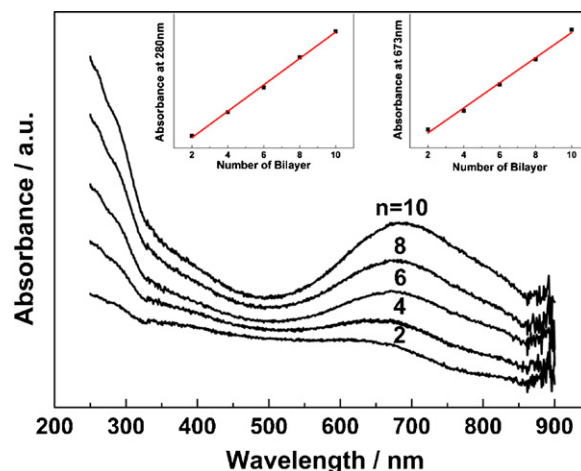

Fig. 3. UV–vis spectra of the deposited (PFIL–GS/PB)$_n$ multilayers ($n = 2, 4, 6, 8,$ and 10). Inset: a plot of absorbance at 280 nm and 673 nm vs. bilayer number.
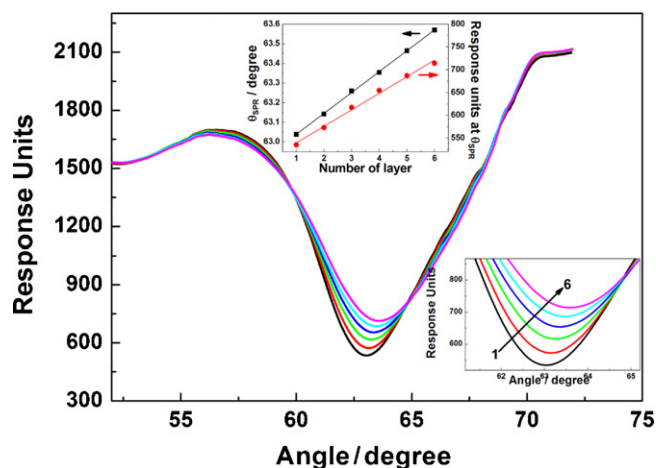
Fig. 4. SPR spectra of the (PFIL–GS/PB)$_n$ multilayer on the gold chip. Inset: the enlarged drawing at SPR dips (below), SPR angle (θ_{SPR}) and response units at θ_{SPR} vs. number of bilayer (above).

SPR spectroscopy has been shown to be a technique of high sensitivity for characterizing ultrathin films at the nanometer thickness scale [35]. In SPR sensor, a surface plasmon is excited at the interface between a metal film and a dielectric medium, the refractive index changes are to be measured. It is known that the SPR dip shifts should be approximately proportional to the changes of refractive index of the solution [36]. Kolomenskii [37] revealed that minute changes in the refractive index of a medium close to the surface of a metal film could be detected owing to a shift in the resonance angle. Kano and Kawata [38] demonstrated that absorption in the sample medium also strongly influences the peak height at the minimum and can even be determined in this way. Therefore, SPR spectroscopy was also employed in the present work to characterize the assembly process of the (PFIL–GS/PB)$_n$ multilayer films to confirm the uniformity of the LBL films. Fig. 4 shows the SPR curves of the LBL films with different bilayer numbers, and the inset presents the linear relationship between the response signal (i.e., the θ_{SPR} (the resonance angle) and the photocurrent response units) and the number of deposited PFIL–GS/PB bilayers. Generally, the θ_{SPR} and the photocurrent response units are correlated with the refractive index of the medium close to the surface of the gold film. In our experiments, the two responses in fact derived from the deposited PFIL–GS and PB NPs. Additionally, this well-defined linear response indicates that the same amount of PFIL–GS and PB NPs were deposited in each cycle, which is consistent with the above-described UV–vis results, thereby leading to a uniform assembly multilayer film.

Scanning electron microscopy (SEM) was also applied to visually inspect the assembly process and confirm the layered structure of the composite. The SEM images were obtained directly on the SPR gold slide without sputter-coated with gold. As shown in Fig. S3 (in the supporting information), it was clear that the amount of irregular graphene sheets which assembled on the gold slide increased with number of the deposited PFIL–GS/PB bilayers increasing. As shown in the expansion image, the PB NPs kept dispersed and absorbed on both the graphene sheets and the gold slide.

3.4. Electrochemical properties of (PFIL–GS/PB)$_n$ multilayer film

H_2O_2 as an important intermediate species or product has been exhibited in many biological and environmental processes. With respect to the high conductivity of PFIL–GS and the excellent electrocatalytic activity toward H_2O_2 of PB, it would be interesting to investigate the possibility of the (PFIL–GS/PB)$_n$ multilayer film
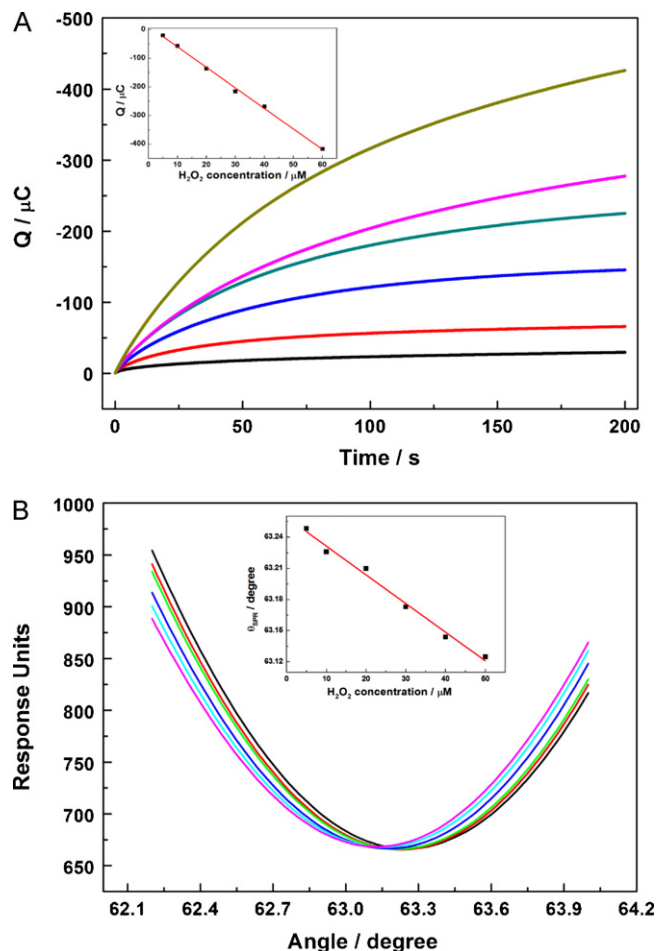

Fig. 5. Electric quantity (A) and SPR angle (θ_{SPR}) (B) changes with different concentration of H_2O_2 in 50 mM PBS solution containing 50 mM PBS (pH = 7.4), applied potential: -0.1 V vs. Ag|AgCl. Inset: calibration as function of H_2O_2 concentration.

for constructing a H_2O_2 electrochemical sensor. The (PFIL–GS/PB)$_n$ multilayer film exhibited high electrocatalytic activity toward reduction of H_2O_2. The Fig. S4 (in the supporting information) compared the electrocatalytic reduction toward H_2O_2 at bare, PB, PFIL–GS, and PFIL–GS/PB modified Au electrodes, respectively. An obvious reduction current at PFIL–GS/PB modified Au electrode clearly indicated that PFIL–GS/PB film had much better electrocatalytical activity toward reduction of H_2O_2 than other cases.

Generally, the surface plasmon optical technique is a powerful tool for characterizing surfaces, interfaces, and thin films. However, it is difficult to detect small molecules with the SPR method owing to the unobvious change in the refractive index. In our system, when SPR is combined with electrochemical technique in situ, H_2O_2 could be indirectly detected via SPR method according to the oxidation state change of PB in the (PFIL–GS/PB)$_n$ multilayer film. Thus, the electrochemical and optical signals could be simultaneously obtained from the composite LBL electrode upon the addition of H_2O_2 because the electroactivity property of the PFIL–GS/PB film enhanced signaling.
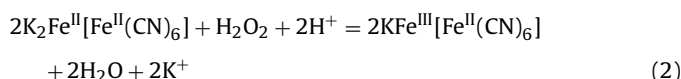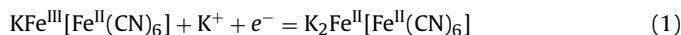
PB has been found to be a good electrocatalyst for the electroreduction of H_2O_2, the cathodic current increases remarkably upon the addition of H_2O_2 at the potential of -0.1 V. A typical current–time (i–t) technique is applied for H_2O_2 sensing. As shown in Fig. 5A, electric quantity, which is obtained by integrating current with time, increases linearly with different concentration of H_2O_2 in a range of 5–60 μM. The fitted linear equation was $y = 11.5 - 7.17x$ ($R = 0.993$), where y and x stand for the electric

Table 1
Results of determination of H_2O_2 in rain water sample.

Rainwater sample	Spike (μM)	Electric quantity		SPR angle change	
		Found (μM)	Recovery (%)	Found (μM)	Recovery (%)
1	15.0	14.43	96.2	15.61	104.1
2	30.0	29.70	99.0	29.04	96.8
3	35.0	34.62	98.9	35.64	101.8

quantity (μC) and the concentration (μM) of H_2O_2. The detection limit for H_2O_2 is found to be 1 μM based on the signal corresponding to three times the noise of the response. To evaluate the reproducibility of this sensor, the electric quantity was determined by 5 successive measurements of 20 μM H_2O_2. And the relative standard deviation (R.S.D.) obtained was 5.48%.

According to the literature [39], the electrocatalytic mechanism of PB for H_2O_2 reduction can be expressed as follows:

$$KFe^{III}[Fe^{II}(CN)_6] + K^+ + e^- = K_2Fe^{II}[Fe^{II}(CN)_6] \quad (1)$$

$$2K_2Fe^{II}[Fe^{II}(CN)_6] + H_2O_2 + 2H^+ = 2KFe^{III}[Fe^{II}(CN)_6]$$
$$+ 2H_2O + 2K^+ \quad (2)$$

Firstly, the PB is reduced to Prussian white (PW) accompanying with the doping of K^+ (Eq. (1)) at the potential of −0.1 V, which caused the SPR angle increased. When inject a certain concentration H_2O_2 into the reaction cell, PW can catalyze the reduction reaction of H_2O_2 (Eq. (2)), and the K^+ liberate the multilayer film at the same time. As the injected concentration of H_2O_2 varies, so does the quantity of K^+ in the assembly multilayer film. The refractive index of the surface modified multilayer film would change with the doping of K^+, associating with the SPR signal changes. As shown in Fig. 5B, the θ_{SPR} is proportional to the different concentration of H_2O_2 in a range of 5–50 μM. The fitted linear equation was $y = 63.3 - 0.00276x$ ($R = 0.999$), where y and x stand for the θ_{SPR} and the concentration (μM) of H_2O_2.

It is well known that dopamine (DA), ascorbic acid (AA), uric acid (UA), Cysteine (Cys), and Glutathione (GSH) often coexist with H_2O_2 in the biological matrix. The typical current-time (i-t) curve was done within a home-made electrochemical reaction cell to evaluated the interferents effect. As shown in Fig. S5 (in the supporting information), it was obvious that the current increased upon the injection of H_2O_2. And no significant interference could be observed for matters, such as DA, AA, UA, Cys and GSH, at concentrations 5 times that of H_2O_2 at 20 μM, indicating these matters coexiting in the sample matrix did not affect the determination of H_2O_2. These results indicated this method was reliable.

The rain water was used for the real sample analysis. The sample without adding H_2O_2 did not show any detectable signal. The recovery was evaluated by comparing the analytic signals of H_2O_2 obtained from the spiked rain water sample with those of the same concentration standard solution (Table 1). The recovery of the spiked samples ranged between 96.2% and 104.1%. And the electrochemical and SPR detection signal were well in accord with each other.

4. Conclusions

In summary, the PFIL–GS composite was synthesized by coupling PFIL through electrostatic and π–π interactions. The introduction of PFIL on the surface of graphene sheets not only produced dispersed CCG, but also provided the building blocks for LBL self-assembly. The (PFIL–GS/PB)$_n$ multilayer films were successfully fabricated by alternately depositing PFIL–GS and PB NPs through electrostatic interactions, and used as substrates of EC-SPR spectroscopy. Upon injecting H_2O_2 into the reaction cell, optical SPR signals and electrochemical current responses were simultaneously monitored in real time. This simultaneous detection method can provide dual information to improve the reliability of the test results, which may offer a new outlook of sensor preparations. Additionally, this study provides a possibility for analyzing the biocatalytic process and amplifying the detection signal of small molecules by SPR spectroscopy.

Appendix A. Supplementary data

Supplementary data associated with this article can be found, in the online version, at doi:10.1016/j.talanta.2011.07.056.

References

[1] D. Li, R.B. Kaner, Science 320 (2008) 1170.
[2] K.S. Novoselov, A.K. Geim, S.V. Morozov, D. Jiang, Y. Zhang, S.V. Dubonos, I.V. Grigorieva, A.A. Firsov, Science 306 (2004) 666.
[3] S. Stankovich, D.A. Dikin, G.H.B. Dommett, K.M. Kohlhaas, E.J. Zimney, E.A. Stach, R.D. Piner, S.T. Nguyen, R.S. Ruoff, Nature 442 (2006) 282.
[4] G.K. Dimitrakakis, E. Tylianakis, G.E. Froudakis, Nano Lett. 8 (2008) 3166.
[5] X. Wang, L. Zhi, K. Mullen, Nano Lett. 8 (2007) 323.
[6] C. Shan, H. Yang, J. Song, D. Han, A. Ivaska, L. Niu, Anal. Chem. 81 (2009) 2378.
[7] N.G. Shang, P. Papakonstantinou, M. McMullan, M. Chu, A. Stamboulis, A. Potenza, S.S. Dhesi, H. Marchetto, Adv. Funct. Mater. 18 (2008) 3506.
[8] A.K. Geim, K.S. Novoselov, Nat. Mater. 6 (2007) 183.
[9] R. Zacharia, H. Ulbricht, T. Hertel, Phys. Rev. B 69 (2004) 155406.
[10] S. Niyogi, E. Bekyarova, M.E. Itkis, J.L. McWilliams, M.A. Hamon, R.C. Haddon, J. Am. Chem. Soc. 128 (2006) 7720.
[11] A.B. Bourlinos, V. Georgakilas, R. Zboril, T.A. Steriotis, A.K. Stubos, C. Trapalis, Solid State Commun. 149 (2009) 2172.
[12] H. Bai, Y. Xu, L. Zhao, C. Li, G. Shi, Chem. Commun. (2009) 1667.
[13] H. Yang, Q. Zhang, C. Shan, F. Li, D. Han, L. Niu, Langmuir 26 (2010) 6708.
[14] J.R. Lomeda, C.D. Doyle, D.V. Kosynkin, W.-F. Hwang, J.M. Tour, J. Am. Chem. Soc. 130 (2008) 16201.
[15] S. Stankovich, R.D. Piner, S.T. Nguyen, R.S. Ruoff, Carbon 44 (2006) 3342.
[16] H. Yang, C. Shan, F. Li, D. Han, Q. Zhang, L. Niu, Chem. Commun. (2009) 3880.
[17] Y. Hu, F. Li, X. Bai, D. Li, S. Hua, K. Wang, L. Niu, Chem. Commun. 47 (2011) 1743.
[18] Y. Shen, Y. Zhang, Q. Zhang, L. Niu, T. You, A. Ivaska, Chem. Commun. (2005) 4193.
[19] Y. Shen, Y. Zhang, X. Qiu, H. Guo, L. Niu, A. Ivaska, Green Chem. 9 (2007) 746.
[20] F. Li, C. Shan, X. Bu, Y. Shen, G. Yang, L. Niu, J. Electroanal. Chem. 616 (2008) 1.
[21] S. Yao, J. Xu, Y. Wang, X. Chen, Y. Xu, S. Hu, Anal. Chim. Acta 557 (2006) 78.
[22] H. Jin, D.A. Heller, M. Kalbacova, J.H. Kim, J.Q. Zhang, A.A. Boghossian, N. Maheshri, M.S. Strano, Nat. Nanotechnol. 5 (2010) 302.
[23] W.W. Chen, B.X. Li, C.L. Xu, L. Wang, Biosen. Bioelectron. 24 (2009) 2534.
[24] Y. Peng, D.L. Jiang, L. Su, L. Zhang, M. Yan, J.J. Du, Y.F. Lu, Y.N. Liu, F.M. Zhou, Anal. Chem. 81 (2009) 9985.
[25] W. Knoll, Annu. Rev. Phys. Chem. 49 (1998) 569.
[26] L. Wang, F. Wang, L. Shang, C. Zhu, W. Ren, S. Dong, Talanta 82 (2010) 113.
[27] W.P. Hu, S.J. Chen, K.T. Huang, J.H. Hsu, W.Y. Chen, G.L. Chang, K.A. Lai, Biosens. Bioelectron. 19 (2004) 1465.
[28] D. Moscone, D. D'Ottavi, D. Compagnone, G. Palleschi, A. Amine, Anal. Chem. 73 (2001) 2529.
[29] G. Decher, Science 277 (1997) 1232.
[30] N.I. Kovtyukhova, P.J. Ollivier, B.R. Martin, T.E. Mallouk, S.A. Chizhik, E.V. Buzaneva, A.D. Gorchinskiy, Chem. Mater. 11 (1999) 771.

[31] D. Li, M.B. Muller, S. Gilje, R.B. Kaner, G.G. Wallace, Nat. Nanotechnol. 3 (2008) 101.
[32] D.M. DeLongchamp, P.T. Hammond, Adv. Funct. Mater. 14 (2004) 224.
[33] G.I. Titelman, V. Gelman, S. Bron, R.L. Khalfin, Y. Cohen, H. Bianco-Peled, Carbon 43 (2005) 641.
[34] S. Stankovich, D.A. Dikin, R.D. Piner, K.A. Kohlhaas, A. Kleinhammes, Y. Jia, Y. Wu, S.T. Nguyen, R.S. Ruoff, Carbon 45 (2007) 1558.
[35] A. Baba, M.-K. Park, R.C. Advincula, W. Knoll, Langmuir 18 (2002) 4648.
[36] X. Yao, J. Wang, F. Zhou, J. Wang, N. Tao, J. Phys. Chem. B 108 (2004) 7206.
[37] A.A. Kolomenskii, P.D. Gershon, H.A. Schuessler, Appl. Opt. 36 (1997) 6539.
[38] H. Kano, S. Kawata, Appl. Opt. 33 (1994) 5166.
[39] D. Du, M. Wang, Y. Qin, Y. Lin, J. Mater. Chem. 20 (2010) 1532.